A STUDY OF FORCED FLOW SEPARATION IN ROCKET NOZZLE

by

J. N. Chiou and R. J. Hung

Final Technical Report

This research work was supported by
the National Aeronautics and Space Administration
George C. Marshall Space Flight Center
Contract NASA/UAH Agreements 5 and 8

The University of Alabama in Huntsville
School of Graduate Studies and Research
P. O. Box 1247
Huntsville, Alabama 35807

July 1974

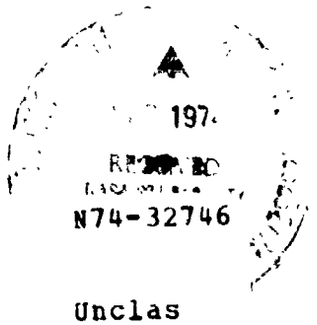

A STUDY OF FORCED FLOW SEPARATION IN ROCKET NOZZLE

by

J. N. Chiou and R. J. Hung

Final Technical Report

This research work was supported by
the National Aeronautics and Space Administration
George C. Marshall Space Flight Center
Contract NASA/UAH Agreements 5 and 8

The University of Alabama in Huntsville
School of Graduate Studies and Research
P. O. Box 1247
Huntsville, Alabama 35807

July 1974

ACKNOWLEDGEMENT

The authors would like to thank Mr. Robert J. Richmond of the Structures and Propulsion Laboratory of NASA/Marshall Space Flight Center, for many stimulative and helpful discussions. They also acknowledge the support of the present study by NASA/Marshall Space Flight Center, through Contract No. NASA/UAH Agreements 5 and 8.

The skillful typing done by Mrs. Carol Holladay is also appreciated.

TABLE OF CONTENTS

.. INTRODUCTION

The operation of a rocket engine at various pressure regions in the combustion chamber results in an uneven side-load in the rocket nozzle before the engine reaches the full operation condition. One solution proposed for preventing the uneven side-load due to the separation of flow, is to use the "trip wires" in the nozzle to create an even forced flow separation and to reduce side-load during the start transient. The purpose of the present study is to investigate the characteristics of flow profile in the rocket nozzle during the start transient, and to examine the possibilities of reducing the side-load thrust by sticking "trip wires" in the nozzle.

To simplify the geometry of flow configuration around the trip wires, we have assumed that the flow is passing through square steps instead of round wires. Since a purely analytic solution is not available at this moment, we have proposed a series of semi-empirical solutions based on the existing literature. In Chapter II, the possible mathematical formulations of the flow parameters, which describe the flow patterns in front of and after the square step, are presented. In Chapter III, the boundary layer thickness and the values of accompanied flow parameters through whole regions of specified nozzle are calculated numerically. In this calculation, th interaction between boundary layer and shock wave has been ignored. The value of boundary layer thickness at the appropriate location of the nozzle is a significant factor for the deisgn of step height in the experimental investigations.

Experimental setup and the model of nozzle used in our experiment, with appropriate steps mounted on the wall of the nozzle, are described in Chapter IV. The experimental results and the discussions are presented in Chapter V.

II. POSSIBLE MATHEMATICAL MODELS

As stated earlier, the nozzle trip wire configuration was proposed to be a potential method for reducing start-transient side loads. Theoretical analysis shows that the side loads are apparently a result of the unsteady, non-uniform flow separation from the wall of the nozzle. Thus, an installation of a device to force a uniform separation should result in a reduction of the magnitude of the side loads. However, a single trip wire would provide the mechanism to control separation at one specific point in the nozzle. As the amount of separation realized depends on the chamber pressure level, it is apparent that more than one trip wire would be required. Therefore, a system of multi-trip wires was chosen.

The basic concept of multi-trip wires is the ability of the flow to snap from one wire to the downstream wire and yet provide a shock of sufficient strength to maintain uniform separation providing the mechanisms for reducing the transient side loads. The problem is how to choose trip wire size and spacing required for each trip wire. Theoretically, these problems are concerned with the study of boundary layer-shock wave interaction in the flow separation associated with recompression in a supersonic nozzle.

In general, boundary layer approach, using continuity, momentum, and energy equations, is used extensively by investigators to solve classical flow separation problems.

$$\frac{\partial \rho}{\partial t} + \frac{\partial}{\partial x}(\rho u_x) + \frac{\partial}{\partial y}(\rho u_y) = 0 \qquad (2\text{-}1)$$

$$\rho\left(\frac{\partial u_x}{\partial t} + u_x \frac{\partial u_x}{\partial x} + u_y \frac{\partial u_x}{\partial y}\right) = -\frac{\partial \rho}{\partial y} + \frac{\partial}{\partial y}\left(\mu \frac{\partial u_x}{\partial y}\right) \qquad (2\text{-}2)$$

$$\rho C_p\left(\frac{\partial T}{\partial t} + u_x \frac{\partial T}{\partial x} + u_y \frac{\partial T}{\partial y}\right) - \left(\frac{\partial P}{\partial t} + u_x \frac{\partial P}{\partial x}\right) = \frac{\partial}{\partial y}\left(K \frac{\partial T}{\partial y}\right) + \mu\left(\frac{\partial u_x}{\partial y}\right)^2 \qquad (2\text{-}3)$$

for compressible two dimensional boundary layer. Here ρ, u, P, T, and C_p denote fluid density, velocity, pressure, temperature and constant pressure specific heat, respectively. Subscripts x and y imply component along x and y directions. Coefficients K and μ are thermal conductivity and viscosity. A complete culation of the boundary layer for a given body with the aid of Equations (2-1) and (2-3) is, in many cases, so

cumbersome and time consuming that it cannot be carried out in practice. It is, therefore, desirable to possess at least approximate methods of solution, to be applied in cases when an exact solution of the boundary layer equations cannot be obtained with a resonable amount of work, even if their accuracy is only limited. Thus, a mean value is obtained from the momentum equation which is derived from Equation (2-2) by integration over the boundary layer thickness. The equation is known as the momentum integral equation of boundary layer theory, or as Von Kármán's momentum integral which is

$$\frac{\tau_w}{\rho} = \frac{d}{dx}\left(U_\infty^2\ \delta^{**}\right) + \delta^*\ U_\infty \frac{dU_\infty}{dx} \qquad (2\text{-}4)$$

for two dimensional incompressible boundary layers. Here

$$\tau_w = \mu \left(\frac{\partial u_x}{\partial y}\right)_{y=0} = \text{shearing stress at the wall}$$

$$U_x = \begin{cases} 0 & \text{for } y = 0 \text{ (at wall)} \\ U_\infty & y = \delta \text{ (outside the boundary layer)} \end{cases}$$

$$\delta^* = \int_0^\infty \left(1 - \frac{u}{U_\infty}\right) dy \quad \text{(displacement thickness)}$$

$$\delta^{**} = \int_0^\infty \frac{u}{U_\infty}\left(1 - \frac{u}{U_\infty}\right) dy \quad \text{(momentum thickness)}$$

To deal with the interaction between an internal dissipative flow and an external nearly isentropic stream such as shock wave interaction with boundary layer, Crocco and Lees[1] generalized the concept of the Von Kármán momentum integral for the dissipative flow region. Mixing between the external and internal streams is admitted as a fundamental physical process, which will furnish the mechanism for pressure rise. This mixing theory is applicable not only for separated and reattached flows, but also for wake flows. One of the most significant discoveries by Crocco and Lees[1] is that in the separation flow the pressure gradient along the surface may reach a maximum at separation and may drop off steeply downstream, and that in reattaching of wake flows the pressure gradient is

negligible some distance upstream of the reattachment point and increases rapidly as this point is approached. In flow separation two governing parameters k and f are defined on the basis of the boundary layer as (Crocco and Lees[1])

$$k = \frac{\delta - \delta^* - \delta^{**}}{\delta - \delta^*} \tag{2-5}$$

and

$$f = \frac{\delta_i \, (\delta_i - \delta_i^* - \delta_i^{**})}{(\delta_i - \delta_i^*)^2} \tag{2-6}$$

where the subscript i denotes the incompressible flow in the Stewartson transformation (Chang[2]).

For laminar and turbulent flows, the separation is characterized by decreasing k and by increasing f. At the separation point, the slope $\partial f/\partial k$ is infinite. This physical picture is essential for separated flow solutions since it gives a clue to the quantitative prediction of what happens after separation. No reliable theoretical solution has been established in this region.

In the practical application, it is assumed that the wire is attached to a flat wall and that the flow is separated on both the upstream and downstream sides of the wire (see Figure 1). Since the wires are small relative to the nozzle diameter, the flow in the region of the wire can be assumed to be planar. Of course, the flow from the throat of the nozzle to the region of first wire is assumed to follow the theory of isentropic expansion. A single oblique shock is taken to occur at the beginning of the front separated region and a second at the downstream edge of the separated base region. Prandtl-Meyer expansion fans were considered to occur at the upper two corners of the wire. The height of the wire is chosen to be comparable to the thickness of the boundary layer. Calculation of the boundary layer thickness in the present study will be shown in the next chapter.

To make the mathematical model tractable, the simplified formulations shown by Chang[2] have been used.

A. <u>Front Step</u>

The pressure coefficient on the front side of the wire is

$$C_p = \frac{2}{\gamma M_1^2} \left(\frac{P_2}{P_1} - 1 \right) \tag{2-7}$$

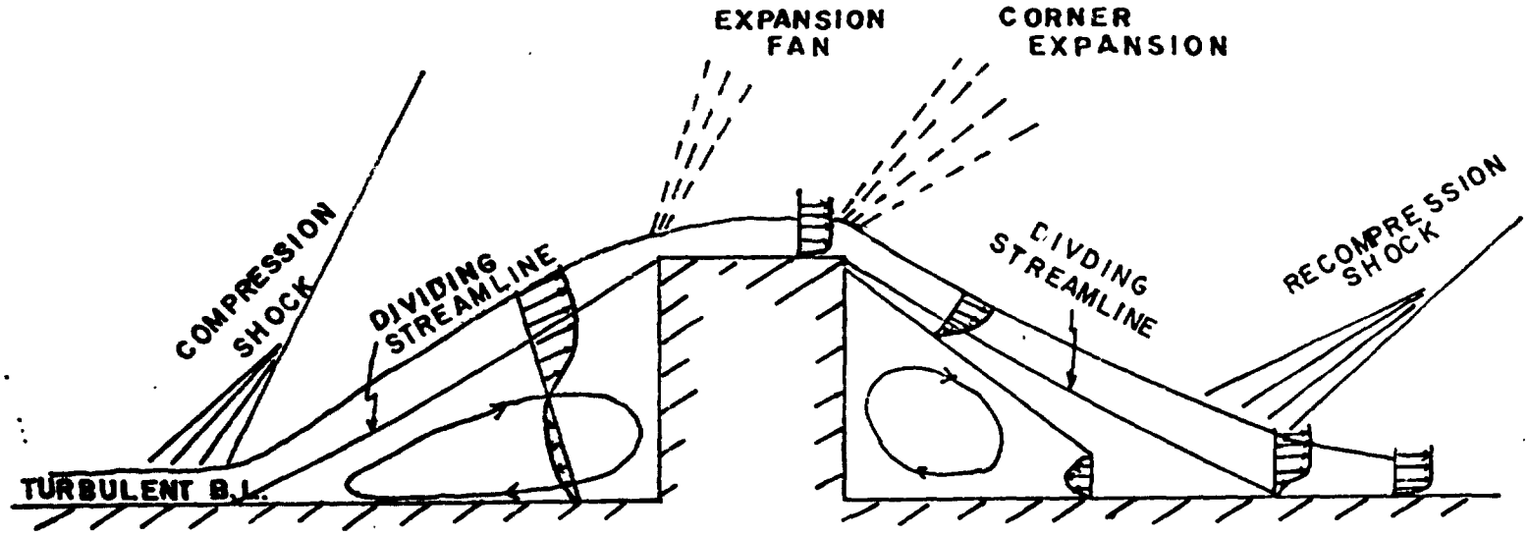

FIG. 1. Flow Configuration Around The Step

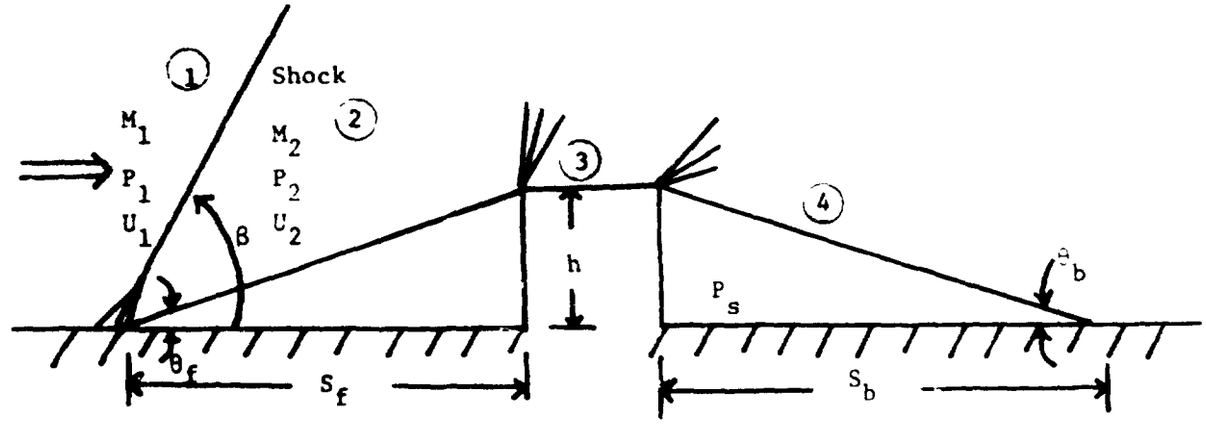

FIGURE 2 REGIONS OF FLOW OF INTEREST AND NOTATION.

where the subscript denotes regions of flow under consideration (see Figure 2).

The relationship among C_p, shock angle resulting fro. separat. region β, and angle of boundary of separated region θ_f, is

$$\tan \theta_f = \frac{\frac{1}{2} C_f \cot \beta}{1 - \frac{1}{2} C_p} \quad . \tag{2-8}$$

Thus, the value of the angle θ_f can be obtained if the shock angle β can be measured from the experiment. The position of the boundary layer separation S_f ahead of the step can be obtained from the following relation

$$S_f = h \cot \theta_f \tag{2-9}$$

where h is the height of step.

B. Back Step

The flow across the regions (2) and (3) can be calculated based on Prandtl-Meyer expansion

$$\nu_2 (M_2) + \theta_2 = \nu_3 (M_3) + \theta_3 \tag{2-10}$$

where $\theta_2 = \theta_f$ and $\theta_3 = 0$. Thus, Equation (2-10) becomes

$$\nu_3 (M_3) = \nu_2 (M_2) + \theta_f \, . \tag{2-11}$$

This provides the Mach number M_3. Furthermore, from momentum equation we can calculate the pressure P_3 as follows:

$$P_3 = P_2 \frac{1 + \gamma M_2^2}{1 + \gamma M_3^2} \quad . \tag{2-12}$$

Again flow across the regions (3) and (4) shall be governed by Prandtl-Meyer expansion. If we use the numerical results computed by Korst[3] in which the results show a good agreement among the experimental data made by Chapman, et al.[4] for the pressure ratio P_3/P_4 against the approaching Mach number (M_3) (See Figure 3), we can calculate the Mach number M_4 based on the following relation

$$M_4 = \frac{1}{\sqrt{\gamma}} \left[\frac{P_3}{P_4} (1 + \gamma M_3^2) - 1 \right]^{1/2} . \qquad (2\text{-}13)$$

Then, the angle of boundary of separated region θ_b can be obtained from Prandtl-Meyer expansion

$$\theta_b = \nu_4 (M_4) - \nu_3 (M_3) . \qquad (2\text{-}14)$$

Therefore, the position of boundary layer separation S_b behind the step can be calculated as follows:

$$S_b = h \cot \theta_b . \qquad (2\text{-}15)$$

Through experiment curve fitting, Herbert and Herd[5] suggested

$$\frac{P_4}{P_s} = 1.15 + 0.05 M_3^2 .$$

Combining with P_3/P_4, as in Figure 3, a plot of S_b/h against M_3 is shown in Figure 4. All notations are defined as in Figure 2. Figure 4 shows that the length of the reattachment decreases with increasing Mach number.

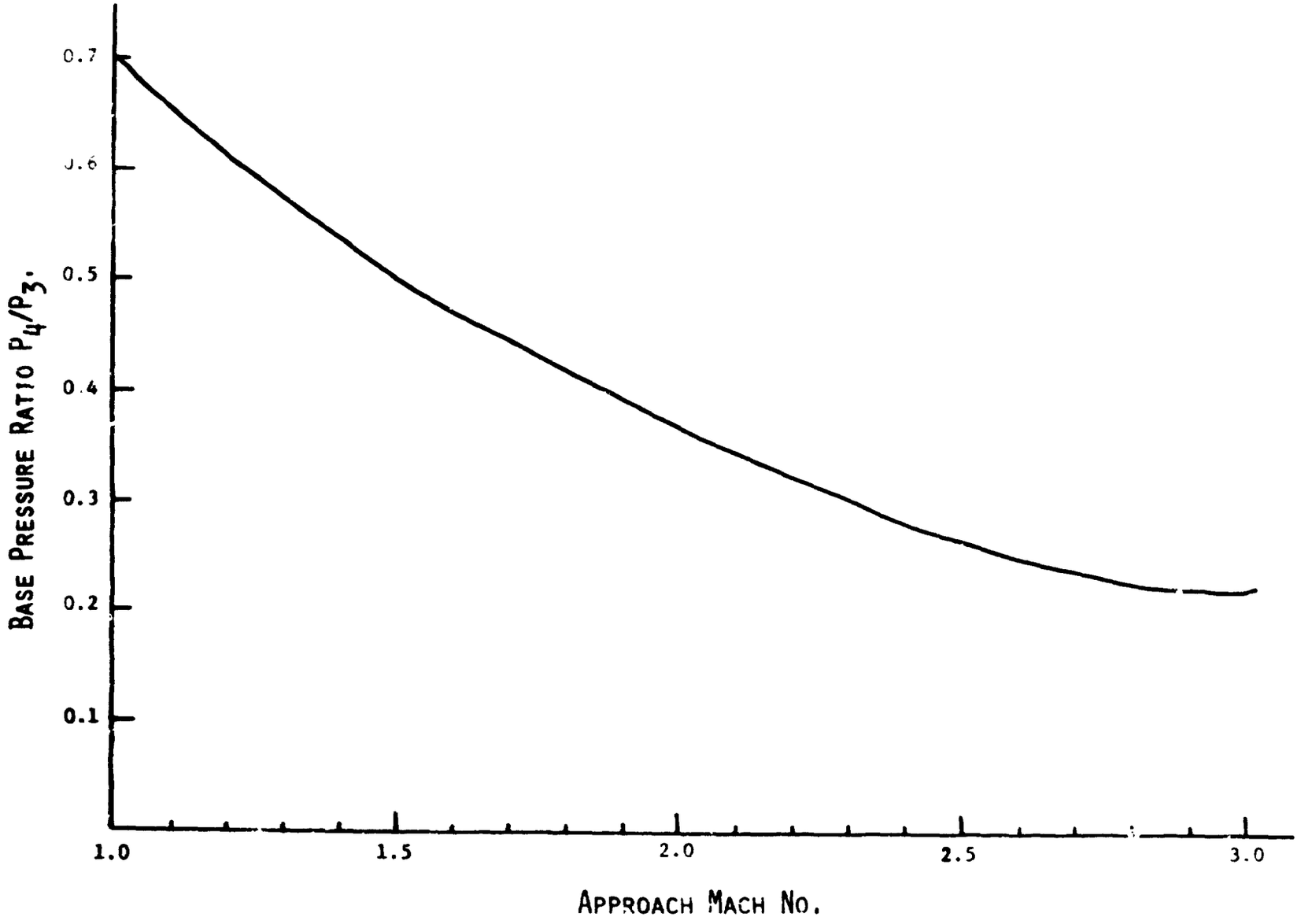

Figure 3 Base Pressure Ratio P_4/P_3 Against Approach Mach No.

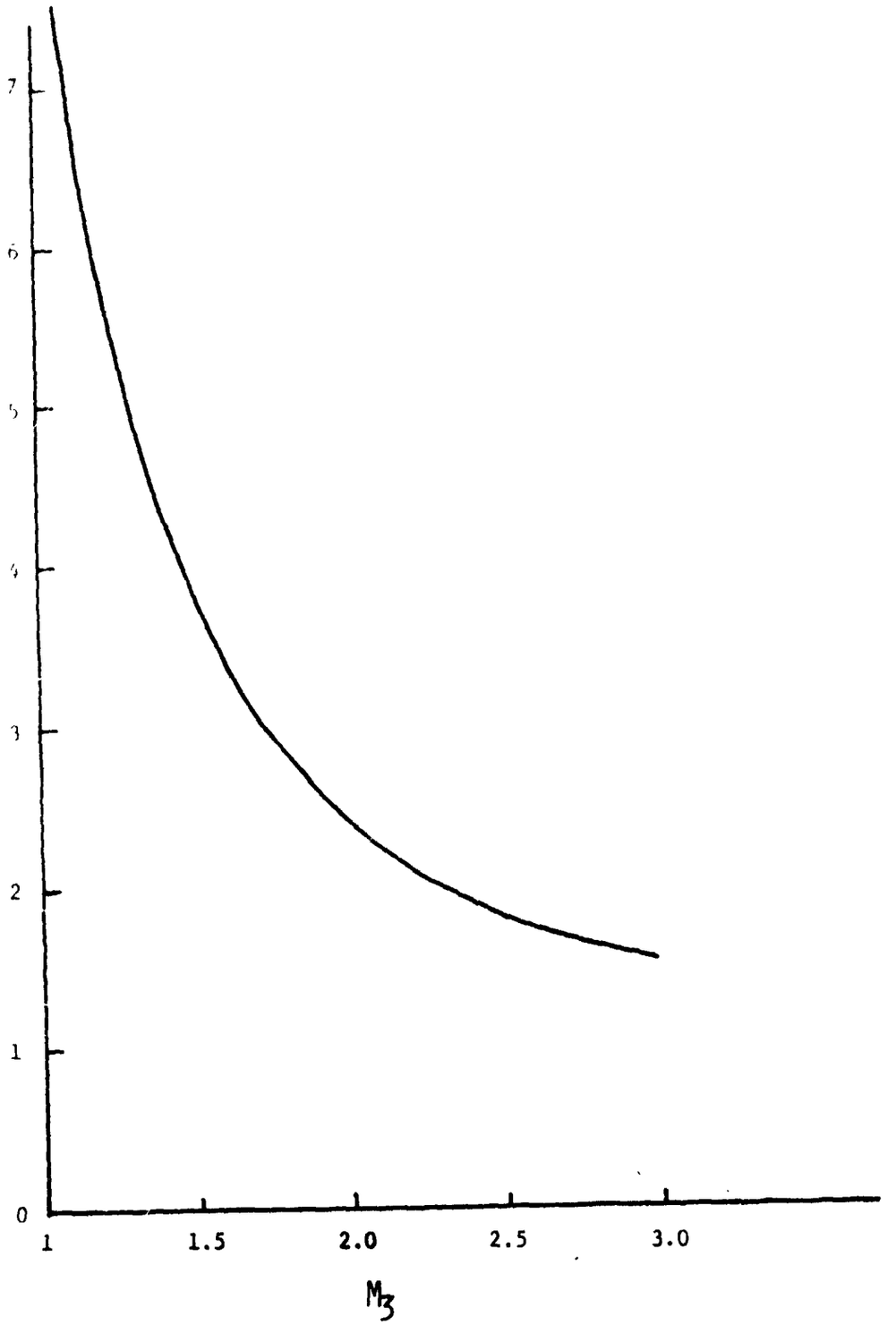

FIGURE 4 BACK STEP REATTACHMENT LENGTH AGAINST M_3.

III. COMPUTATION OF BOUNDARY LAYER THICKNESS

The computation of boundary layer, in general, shall follow the theory of boundary layer developed by Prandtl. However, Von Kármán integral momentum equation is more suitable for practical application to engineering problems. In this section, we use the integral momentum and energy equations in axisymmetric form for compressible boundary layer flow. The governing equations are as follows:

$$\frac{d\delta^{**}}{dx} = \frac{C_f}{2}\left[1 + \left(\frac{dr}{dx}\right)^2\right]^{1/2} - \delta^{**}\left[\frac{1 + \frac{\delta^*}{\delta^{**}}}{U_\infty}\frac{dU_\infty}{dx} + \frac{1}{\rho_\infty U_\infty}\frac{d(\rho_\infty U_\infty)}{dx} + \frac{1}{r}\frac{dr}{dx}\right] \tag{3-1}$$

for integral momentum equation, and

$$\frac{d\phi}{dx} = C_H\left[\frac{H_{aw} - H_w}{H_o - H_w}\right]\left[1 + \left(\frac{dr}{dx}\right)^2\right]^{1/2} - \phi\left[\frac{1}{\rho_\infty U_\infty}\frac{d(\rho_\infty U_\infty)}{dx} + \frac{1}{r}\frac{dr}{dx} + \frac{1}{H_o - H_w}\frac{d(H_o - H_w)}{dx}\right]$$

for integral energy equation. Here, the displacement thickness δ^*, momentum thickness δ^{**} and energy thickness ϕ for the compressible flow are identified as follows:

$$\delta^* = \int_0^\delta \left(1 - \frac{\rho u}{\rho_\infty U_\infty}\right) dy$$

$$\delta^{**} = \int_0^\delta \frac{\rho u}{\rho_\infty U_\infty}\left(1 - \frac{u}{U_\infty}\right) dy$$

and

$$\phi = \int_0^\delta \frac{\rho u}{\rho_\infty U_\infty}\left(1 - \frac{h_o - H_w}{H_o - H_w}\right) dy \ .$$

The skin friction coefficient is defined as

$$C_f = \frac{2\tau_o}{\rho_\infty U_\infty^2}$$

which has a form of Blasius relation

$$C_f = \frac{0.025}{(Re_{\delta^{**}})^{0.25}}$$

where the Reynolds number in terms of momentum thickness is

$$Re_{\delta^{**}} = \frac{\rho_\infty U_\infty \delta^{**}}{\mu_\infty} .$$

The Stanton number is defined as

$$C_H = \frac{\dot{q}_w}{\rho_\infty U_\infty (H_{aw} - H_w)}$$

which can be shown in the following form

$$C_H = \frac{\frac{C_f(Re_\phi)}{2}\left(\frac{\phi}{\delta^{**}}\right)^n}{1 - 5\frac{C_f(Re_\phi)^{1/2}}{2}\left(1 - P_r + \ell n \frac{6}{5P_r+1}\right)} .$$

Velocity and enthalpy profiles across the boundary layer are assumed to follow the relationships:

$$\frac{u}{U_\infty} = \left(\frac{y}{\delta}\right)^{\frac{1}{n}} \quad \text{for} \quad y \le \delta$$

$$\frac{h_o - H_w}{H_o - H_w} = \left(\frac{y}{\delta'}\right)^{\frac{1}{n}} \quad \text{for } y \le \delta'$$

$$\frac{u}{U_\infty} = 1 \quad \text{for } y > \delta$$

$$\frac{h_o - H_w}{H_o - H_w} = 1 \quad \text{for } y > \delta' .$$

where δ and δ' are momentum and thermal boundary layer thicknesses, respectively. The definition of enthalpy is

$$H = \int_o^T C_p \, d\,T$$

$$h_o = H + \frac{u^2}{2}$$

$$H_w = \int_o^{T_w} C_p \, d\,T \quad .$$

The adiabatic wall enthalpy H_{aw} is defined as

$$\frac{H_{aw}}{H_o} = \frac{H_\infty + (P_r)^{1/3} \frac{U_\infty^2}{2}}{H_\infty + \frac{U_\infty^2}{2}} \quad .$$

The density ρ within the boundary layer is obtained from the perfect gas equation, assuming the pressure is constant across the boundary layer

$$\frac{\rho}{\rho_\infty} = \frac{T_\infty}{T} \quad .$$

The computer calculation is carried out through the programming made by Omori et al.[6]. The results are shown in Figure 8.

IV. APPARATUS AND MODELS

A. Apparatus

The set up of the experiment is shown in Fig. 5 and Fig. 6. A schematic diagram of the flow system is shown in Fig. 7. Flow pictures were taken by using a differential interferometer which is also shown in Fig. 7. The test section was 1.8" x 2.1". The compressed air was stored in a 300 cubic feet tank which allowed the reservoir pressure to be maintained at 600 psig during the entire test.

B. Experimental Model

The shape of the model is shown in Fig. 8. It is 2.86" long and 0.8" wide. The upper part of the nozzle was fixed. In order to change step heights easily for different tests, the lower part of the model was made removable. Slots of depth of 0.025" were cut in the model for the step to be mounted. The location of the slots are 0.75", 1.055", and 1.358" from the end of the nozzle exit, respectively.

The heights of the step were made 0.027, 0.033, 0.035, 0.039, 0.045, 0.051, and 0.057 inches which gave the step heights 0.002, 0.006, 0.008, 0.014, 0.020, 0.026 and 0.032 inches when plugged into the slot of the model. Thus, we were able to use different step heights between 0.002 and 0.032 inches, which covered the range of both lower and higher than the boundary layer thickness in the test sections.

In the later test of two or three step experiments, models were cut two or three slots at proper position chosen. All possible bleed passages were sealed with sealant. A small air bleeding was used to prevent formation of fog on the window of the test section.

FIG. 5 EXPERIMENT SETUP

FIG. 6 EXPERIMENT SETUP (DIFFERENT VIEW ANGLE).

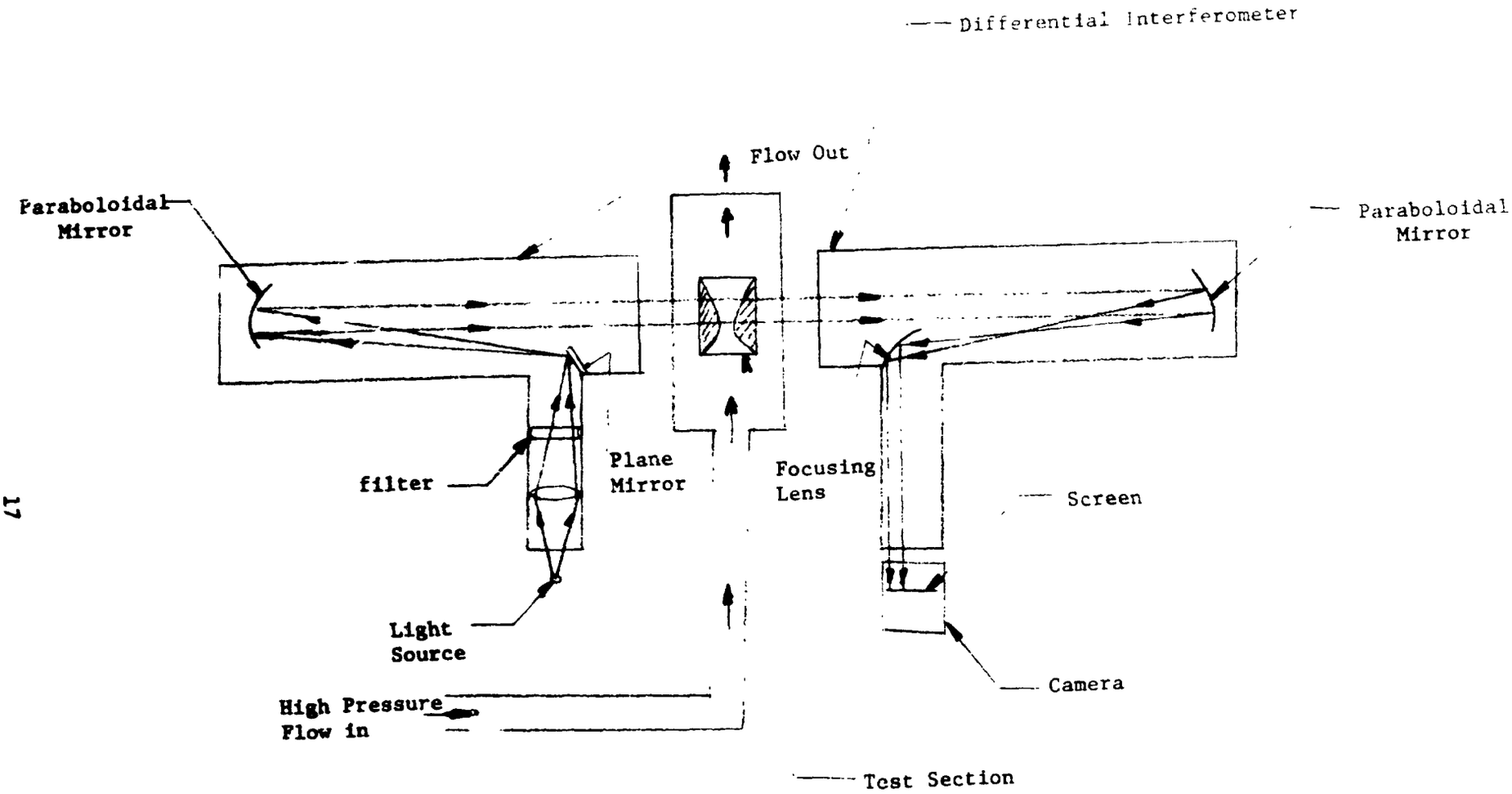

FIG. 7. Schematic Diagram of the Flow System

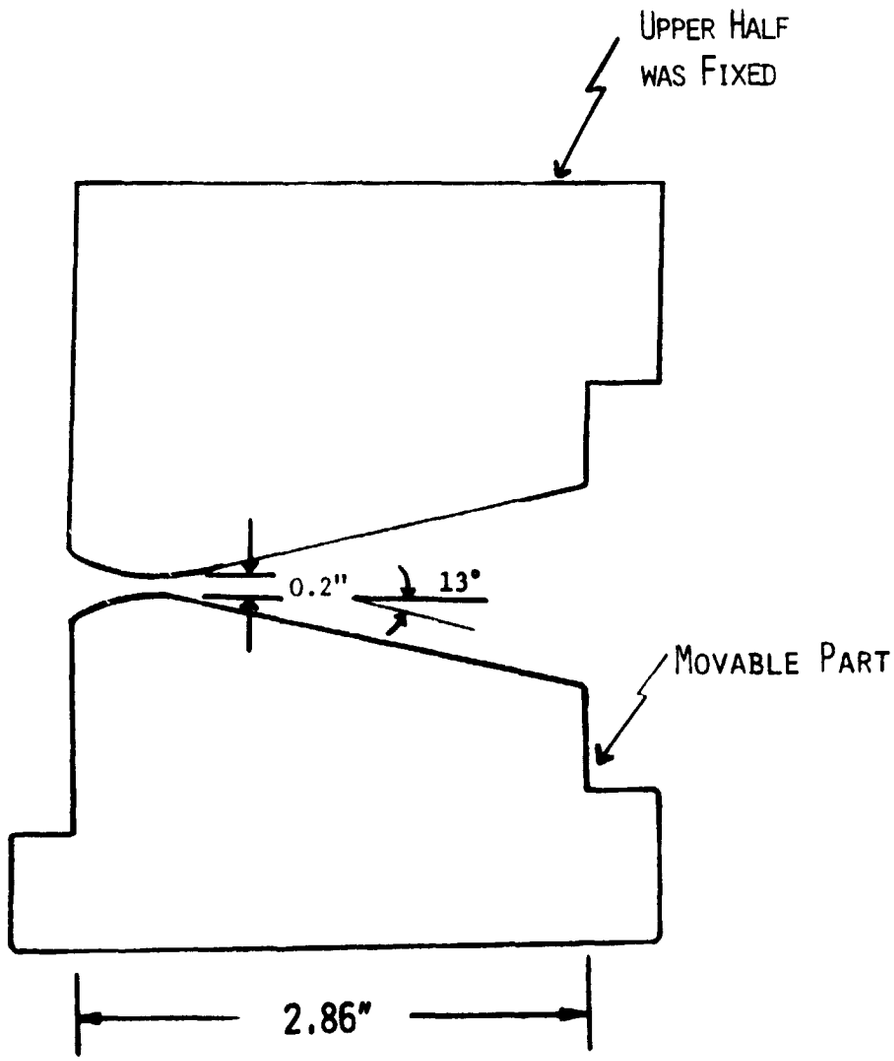

FIGURE 8. SHAPE OF MODEL

V. TEST PROGRAM

In order to simulate the start transient condition of rocket engine in the present test program, the chamber pressure was increased from zero psig to normal operation pressure up to about 300 psig which allowed expansion nozzle exit Mach numbers up to ~ 3.5. The test procedure is to introduce the high pressure gas into chamber gradually and increase the gas flow rate pasing through the expansion nozzle. During the test, we have observed how the shock was formed and passed over the steps, and how it propagated out of the nozzle when both gas pressure and flow rate were increased. The flow parameters along the nozzle, such as temperature, pressure, density, velocity, Mach number and boundary layer thickness, are shown in Fig. 9. Photographs were taken in order to determine the natural separation points at various pressures. These are needed for the calculation of the ratio of separation pressure to ambient pressure.

Single step experiments were carried out by inserting various step heights into the slots at three different positions as previously described. For each test case, reservoir pressure at the moment the shock attached to the step and at the moment the flow reattached after flow separation, were recorded. The purpose of these experiments was to determine how much increase in reservoir pressure is needed for the flow to reattach after being force-separated by the existence of the step. Tests included both change of step heights and step positions. Step heights used were 0.002, 0.008, 0.014, 0.020, 0.026, and 0.032 inches. Steps were placed at 0.75, 1.055, or 1.358 inches from the end of the model.

To study the change of reservoir pressures needed between flow separation and reattachment for multi-step conditions, two-step and three-step cases were also tested. In two-step cases, steps were placed at the positions 0.75 and 1.358 inches from the end of the model, and step heights used were 0.002, 0.006, 0.010, 0.020, and 0.032 inches. In three-step cases, the positions of the steps were 0.75, 1.055, and 1.358 inches from the end of the model and step height chosen was 0.032 inches. Again, the reservoir pressures were recorded at the time the

flow separated at the step and when the flow reattached after the shock moved downstream.

The next point of natural separation after the reattachment of flow on each step was determined photographically.

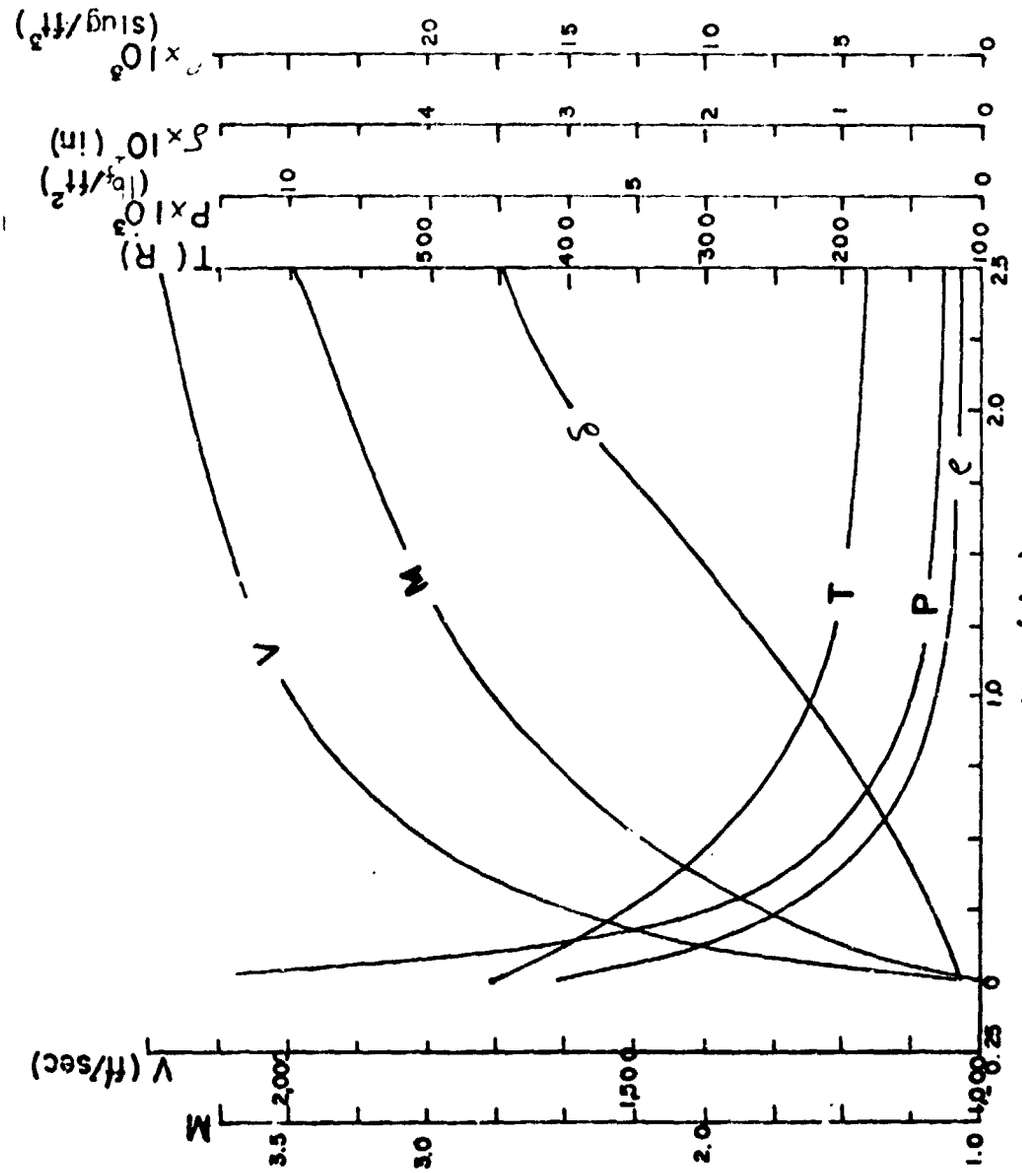

Fig. 9 Flow Parameters Along Nozzle

VI. RESULTS AND DISCUSSIONS

Points of natural separation versus chamber pressures are shown in Fig. 10. The relation appears to be linear which means that the increase reservoir pressure results in pushing the point of natural separation further out. It was also found that the ratios of pressure at the point of separation and the atmospheric pressure are ranging from 0.5 to 0.41 for the range of reservoir pressure from 70 to 220 psig.

In Table I, reservoir pressures, at the time the shock attaches to the step and the flow reattaches after the flow separation due to the step, are listed for different step heights and three different positions (0.75", 1.055" and 1.35" from the exit of nozzle). Local static pressures before the shock and after flow reattachment corresponding to P_{01}'s and P_{02}'s, are also listed. The static pressure difference needed for the shock to jump over the step was found statistically to be about 2.5 psi. Figure 11 shows the ratio of local pressure just before flow separation (P_1) to that of local pressure just after flow reattachment (P_2) as a function of step height. Figure 11 also shows that this ratio increases drastically at $h/\delta \approx 1$. Table II shows the ratios of local pressure to ambient pressure at the point of separation when the flow reattached. It is interesting to point out that the pressure ratio is about 0.9, which is much higher than the case without the step. From the photographic measurement, the distance from the flow reattachment to the step to the next point of natural separation is 10 times the height of the step.

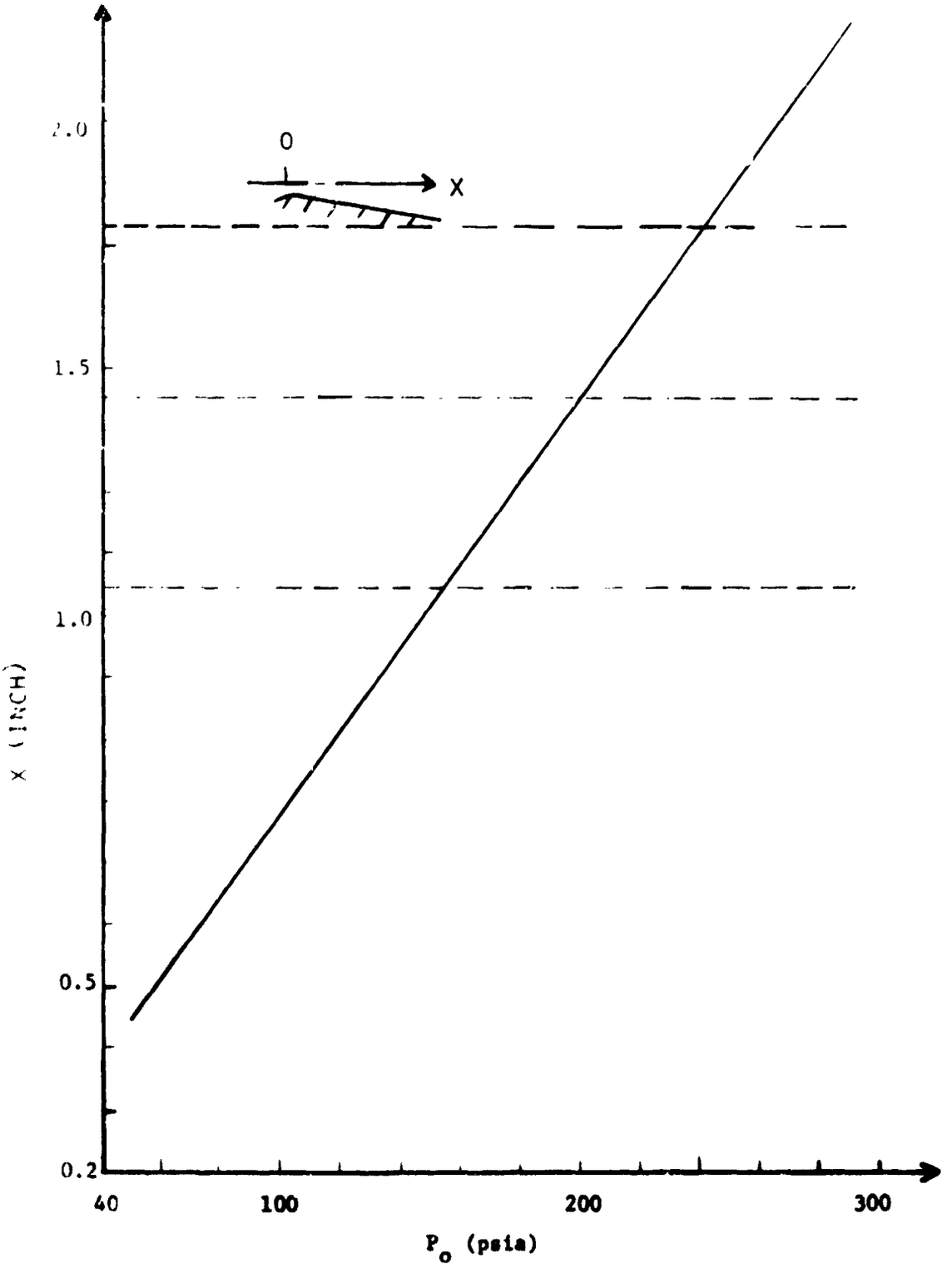

FIGURE 10. RESERVOIR PRESSURE VS. DISTANCE OF NATUAL SEPARATION FROM THE THROAT (UAH MODEL).

P_1: Static pressure before shock as the shock attaches to the step.

P_2: Static pressure before shock as the flow reattaches after separation shock moves downstream.

h: Step height

δ: Boundary layer thickness.

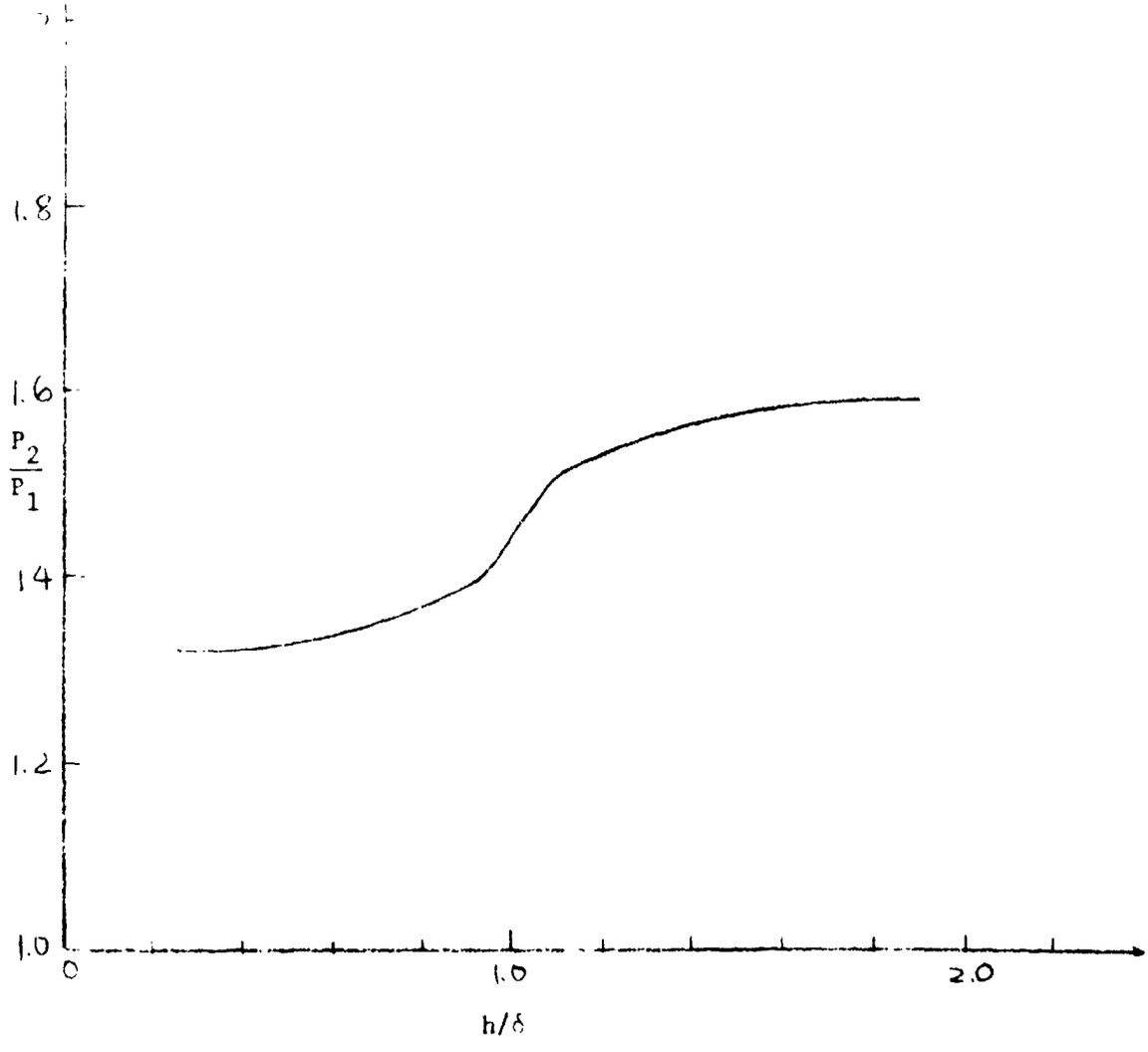

Fig. 11. P_2/P_1 Versus Step Height (h/δ).

TABLE I. PRESSURE DATA FOR SINGLE STEP CASES

	Step Height 1/1000"	P_{01} psia	P_{02} psia	P_1 psia	P_2 psia	$\Delta P=P_2-P_1$ psi
Step Close to Exit	27	190	290	5.434	8.294	2.86
	21	170	264	4.862	7.550	2.688
	15	175	280	5.005	8.008	3.003
	9	180	255	5.148	7.293	2.145
Step at Middle	32	135	215	4.974	7.922	2.948
	26	145	236	5.343	8.696	3.353
	20	150	220	5.527	8.107	2.580
	14	160	218	5.896	8.033	2.137
	8	165	220	6.080	8.107	2.027
	2	174	219	6.411	8.070	1.659
Step Close to Throat	32	120	170	6.348	8.993	2.645
	26	119	163	6.295	8.622	2.327
	20	119	167	6.295	8.834	2.539
	14	119	175	6.295	9.257	2.962
	8	123	170	6.506	8.993	2.487
	2	122	171	6.452	9.045	2.592

P_{01}: Reservoir pressure when the shock attaches to the step.

P_{02}: Reservoir pressure when the flow reattaches after separation by the step.

P_1, P_2: Local static pressure corresponding to P_{01} and P_{02}, respectively.

Step close to the exit: 0.75" from the exit.

Step at middle: 1.055" from the exit.

Step close to throat: 1.358" from the exit.

TABLE II. NATURAL SEPARATION PRESSURE AFTER REATTACHMENT OF FLOW

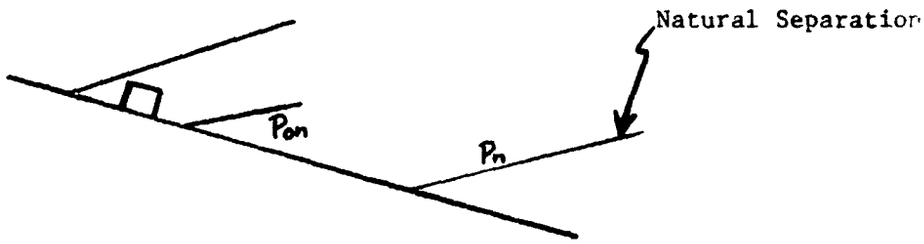

Step Height (inches)	P_{on} (psia)	$\frac{P_n}{P_a}$	$\frac{P_{on}}{P_a}$
0.032	136.9	.87	9.31
0.026	131.6	.84	8.95
0.020	136.6	.89	9.29
0.014	145.0	.908	9.86
0.008	142.6	.906	9.7
0.002	143.9	.92	9.79

where

P_{on} = calculated total pressure for the flow region after the shock reattachment.

P_n = calculated local pressure at the location where natural separation occurred.

P_a = ambient atmospheric pressure.

Tables III and IV show the variation of chamber pressures during the experiment for the cases of two-steps and three-steps, respectively. Figures 12, 13, 14, and 15 show the typical flow pictures of natural separation for the cases of single-step, two-steps, and three-steps, respectively. The photographic pictures were taken by using a differential interferometer.

On the average, it is noted that within the range of Mach numbers tested, the distance from the point of flow separation in front of the step to the step is about 3 to 5 times that of the step height; and the distance from the step to the point of reattachment downstream is about twice the step height.

TABLE III. PRESSURE DATA FOR TWO-STEP CASES

Step Heights	Step No.	P_{01} psia	P_{02} psia	P_1	P_2	$\Delta P=P_2-P_1$	$\frac{P_{02}}{P_{01}}$
32 / 1000"	1	120	170	6.348	9.257	2.909	1.46
	2	230	250	34.13	37.09	2.97	1.09
20 / 1000"	1	120	165	6.348	8.728	2.38	1.38
	2	225	245	33.38	36.35	2.96	1.09
10 / 1000"	1	120	163	6.348	8.622	2.274	1.36
	2	220	240	31.46	34.32	2.86	1.09
6 / 1000"	1	125	170	6.612	8.943	2.381	1.36
	2	200	220	30.36	33.8	2.82	1.10

Steps at 0.75" and 1.358" from the Exit.

TABLE IV. PRESSURE DATA FOR THREE-STEP CASES

Step No.	P_{01} psia	P_{02} psia	P_1 psia	P_2 psia	$\Delta P = P_2 - P_1$ psi
1	113	195	5.977	10.31	4.333
2	195	229	14.85	18.27	3.42
3	229	295	16.02	20.64	4.62

Three Steps:

Steps at 0.75", 1.055", and 1.358" from the exit.

Step height 32/1000".

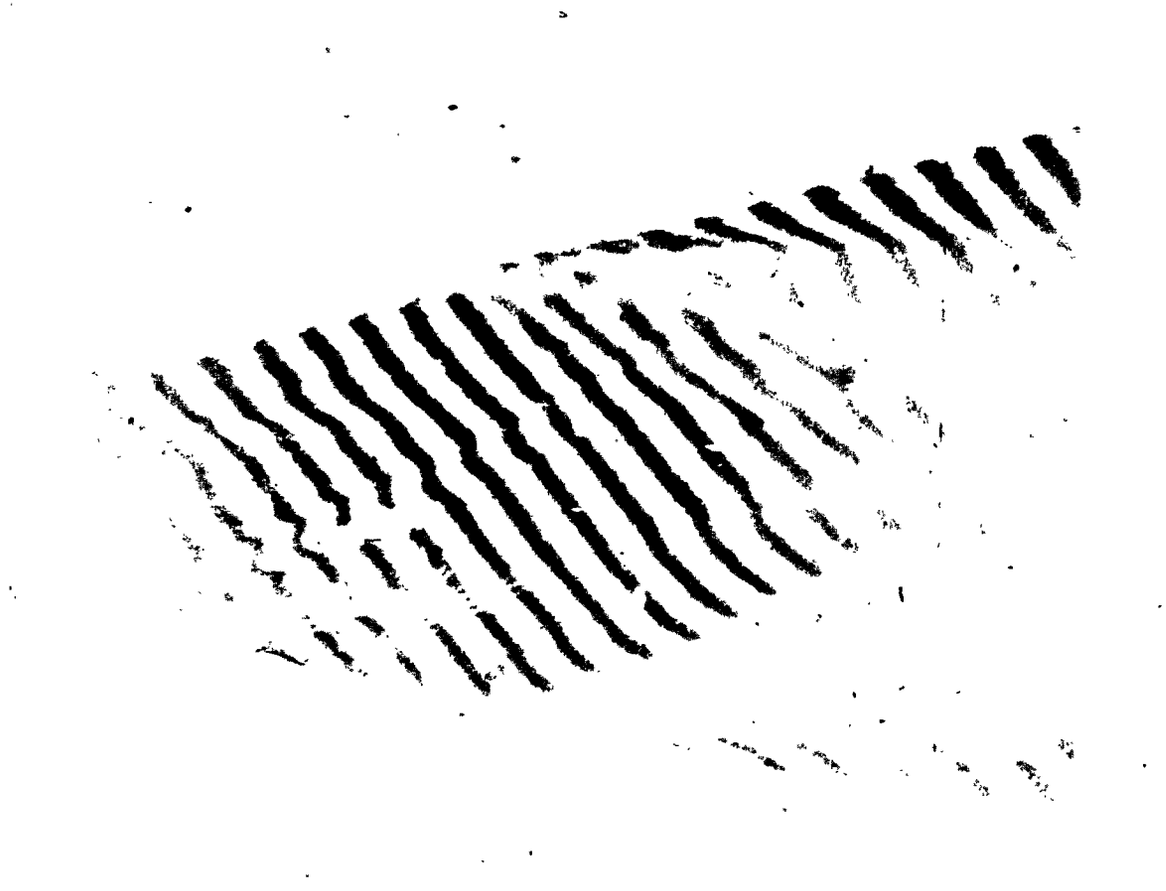

Figure 12. Typical Flow Picture of Natural Separation.

Figure 13. Typical Single-Step Flow

Figure 14. Typical Two-Step Flow

Figure 15. Typical Three-Step Flow.

REFERENCES

1. Crocco, L. and Lees, L., "A Mixing Theory for the Interaction Between Dissipative Flows and Nearly Isentropic Streams," J. of the Aeronautical Science 19, pp. 649-676, 1952.

2. Korst, H. H., Page, R. H., and Childs, M. E., "A Theory Base Pressure in Transonic and Supersonic Flow," Univ. of Illinois Experiment Station, March 1955, also ASME Paper 56-AMP-30, 1956.

3. Chang, P. K., "Separation of Flow," Pergamon Press, Oxford, London, 1970.

4. Chapman, I. R., Wimbrow, W. R., and Kester, R. H., "Experimental Investigation of Base Pressure on Blunt Trailing-Edge Wings at Supersonic Velocities," NACA TN 2611, 1952.

5. Herbert, M. V. and Herd, R. J., "Boundary-Layer Separation in Supersonic Propelling Nozzles," N.G.T.E., Report No. R260.

6. Omori, S., Gross, K. W., and Krebsbach, A., NASA Technical Note, TN D-6825, 1972.